Advancing data analysis for reflectivity measurements of holographic nanocomposite gratings

2016 J. Phys.: Conf. Ser. 746 012022

(http://iopscience.iop.org/1742-6596/746/1/012022)

Advancing data analysis for reflectivity measurements of holographic nanocomposite gratings

Jürgen Klepp[1,*], Christian Pruner[2], Yasuo Tomita[3], Peter Geltenbort[4], Joachim Kohlbrecher[5] and Martin Fally[1]

[1]Faculty of Physics, University of Vienna, Boltzmanngasse 5, A-1090 Vienna, Austria
[2]Department of Materials Science and Physics, University of Salzburg, Hellbrunnerstrasse 34, A-5020 Salzburg, Austria
[3]Department of Engineering Science, University of Electro-Communications, 1-5-1 Chofugaoka, Chofu, Tokyo 182-8585, Japan
[4]Institut Laue-Langevin, 71 avenue des Martyrs, 38000 Grenoble, France
[5]Laboratory for neutron scattering, Paul Scherrer Institut, 5232 Villigen PSI, Switzerland

E-mail: *juergen.klepp@univie.ac.at

Abstract. We discuss the analysis of neutron rocking curves measured with holographic nanoparticle-polymer composite gratings with SANS instruments and at very-cold neutron beamlines. In particular, the effects of broad incident wavelength-distributions and of nonuniformity of the refractive-index profile along the grating depth are assessed.

1. Introduction

Photosensitive materials in combination with holographic techniques can be used to produce diffraction gratings for neutron-optics. One-dimensional sinusoidal holograms recorded in such materials exhibit a periodic light- and neutron-refractive-index pattern arising from a light-induced density modulation. They work as diffraction gratings. The recorded refractive-index pattern is described by $n(x) = n_0 + \Delta n_1 \cos(2\pi x/\Lambda)$, where n_0, Δn_1 and Λ are the mean refractive index, the refractive-index modulation amplitude and the grating period, respectively. $\Delta n_1 = \lambda^2 b_c \Delta\rho/2\pi$ for neutrons, with the scattering-length density modulation amplitude $b_c\Delta\rho$. Examples for such materials already tested with neutrons are deuterated (poly)methylmethacrylate [1, 2, 3, 4, 5], holographic polymer-dispersed liquid crystals [6, 7] and nanoparticle-polymer composites (NPCs, see [8, 9, 10, 11] and Fig. 1).

A decisive advantage of holographic NPC gratings is their versatility due to the range of possible choices of nanoparticle composition, thereby selecting the most suitable value of the coherent scattering length/absorption cross section for a specific application. For instance, magnetic or absorptive terms could be added to the periodic optical potential by incorporating ferromagnetic/superparamagnetic [12] nanoparticles or Gd-based nanoparticles, respectively. Magnetic grating-structures could be used as polarizing beam splitters for retrofitting small-angle neutron scattering (SANS) instruments. Absorption gratings with small Λ could find applications in very-cold neutron (VCN) interferometry [13]. Recently investigated material types [14, 15] exhibited an increase in reflectivity of about 40% as compared to earlier experiments.

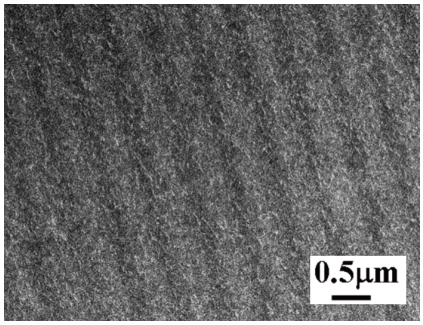

Figure 1. A transmission electron microscope image of the cross section of a plane-wave grating recorded in a ZrO_2 NPC sample at grating spacing of 0.6 μm. Note that the darker portions in the image correspond to ZrO_2 nanoparticle rich regions, indicating holographic assembly of nanoparticles in the formed polymer [9, 10].

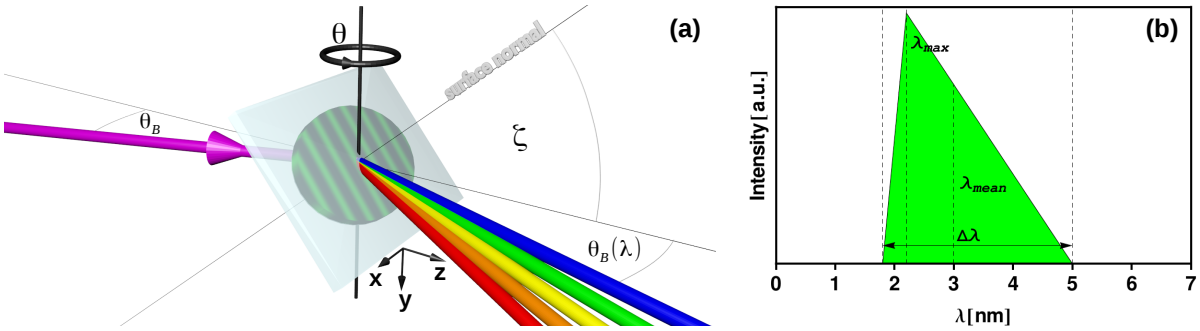

Figure 2. (a) Sketch of the experimental setup. (b) Our model of the asymmetric wavelength distribution of PF2VCN.

Measured reflectivity curves ('rocking curves', i.e., neutron reflectivity vs. angle of incidence) of NPC gratings are usually fitted using the theoretical models by Kogelnik [16] or the equivalent dynamical diffraction theory (DDT) [17, 18]. For gratings with grating-strength decaying exponentially along the direction of the grating thickness, Uchida's approach [19] is applied. For similarities and differences between the approaches, see Refs. [20, 21, 22, 23], for instance.

In comparison to crystal neutron optics it should be noted that NPC gratings are usually designed to work as relatively thin (in an optical sense [24]) diffraction gratings: In some cases, more than two diffraction spots can be visible for a given angle of incidence, so that the two-beam approximation is not applicable. In that case, the so-called rigorous coupled-wave analysis (RCWA) [20, 25, 26], that accounts for an arbitrary number of, even overlapping, peaks must be adopted for data analysis. Furthermore, the Pendellösungs length of NPC gratings can be of the order of 1 mm, so that the oscillatory structure of rocking curves is observable with realistic beam collimation. As a consequence, and most importantly, it is possible to beat the usual limit of about 50% that is imposed on the reflectivity of thick crystals in Laue (transmission) geometry by the mere fact that measured rocking curves are usually smeared out over a vast number of reflectivity oscillations [17]. In contrast, NPC gratings can in principle reach mirror-like reflectivity and even exhibit full Pendellösung oscillations as a function of angle of incidence θ, neutron wavelength λ, scattering length density modulation amplitude $b_c\Delta\rho$ or grating thickness d [27, 28, 29, 30, 31]. DDT predicts that—due to the particular superposition state within a periodic structure—the neutron intensity oscillates between reflected and transmitted beams

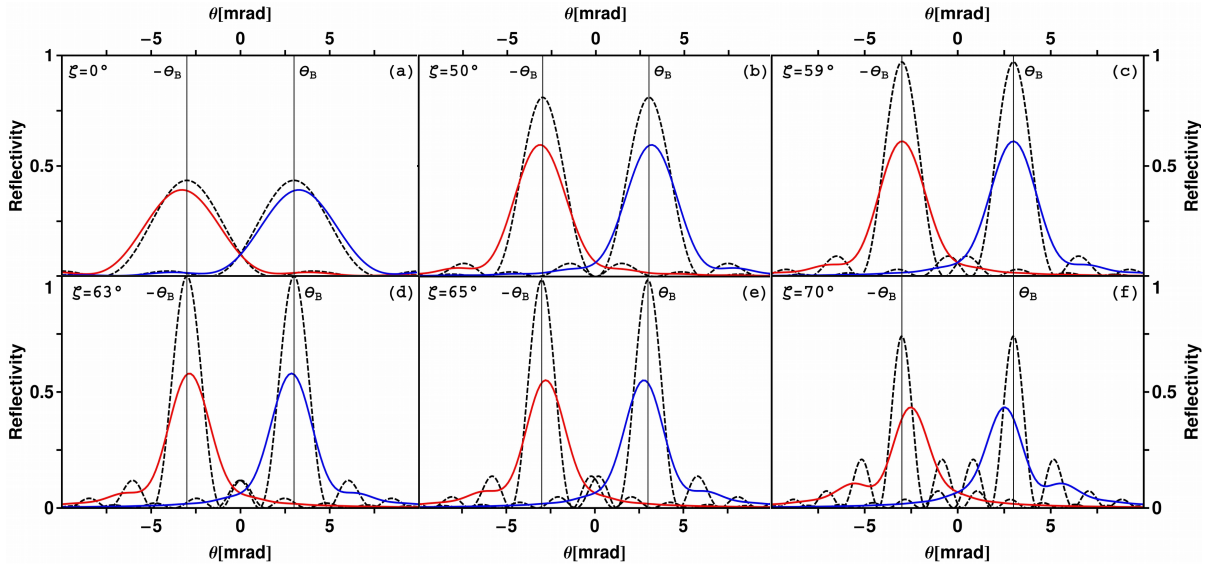

Figure 3. Theoretical rocking curves calculated using DDT (dashed lines) and convolutions of DDT with a slit function (determined by the collimation) and the wavelength distribution shown in Fig. 2, for various tilt angles (a) – (f).

(Pendellösung interference). It has been shown that NPC gratings can be used as 50:50 beam splitters [32, 33], mirrors [34] or three-port beam splitters (30:30:30) [35] for cold- and very-cold neutrons (VCN). Furthermore, in the course of the experiments described in the above references, it has been asserted that the grating properties and quality have not changed substantially for many years, with the NPC gratings stored under ambient conditions.

In the present paper, some issues arising in the data analysis of reflectivity measurements with NPC gratings, related to the above facts, are discussed.

2. A typical experiment

In Fig. 2 (a), a schematic of the experimental setup used at the VCN beam position of the ILL (PF2VCN) is shown: We use a collimated beam with divergence limited both horizontally and vertically to about 10^{-3} rad. The collimation allows to observe the side maxima of the rocking curves at reasonable flux. The wavelength spectrum of the incident beam is very broad and asymmetric at PF2VCN, as shown in Fig. 2 (b) (for a measured VCN spectrum see, for instance, [13]). The cut-off at shorter wavelengths is due to reflection from a neutron (super)mirror used to redirect the incident beam, while the large width is due to the spectrum originating from the vertical and curved guide that feeds the ultra-cold neutron turbine [36]. Of course, further shaping of the incident spectrum is possible, but making use of the entire incident flux is preferable. Since, according to the Bragg equation $\lambda = 2\Lambda \sin\theta_B$ and due to gravity, longer λ means larger Bragg angles $\theta_B(\lambda)$ and lower impact positions on the detector (for given sample-detector distance), respectively. The longer λ, the further away from the 0^{th} diffraction order spot (both horizontally and vertically) do diffracted neutrons hit a subsequent 2D detector at a particular distance from the grating. Consequently, we can discriminate the (mean) wavelengths on the 2D detector (pixel-size $\approx 2 \times 2\,\text{mm}^2$) at about 2 m sample-detector distance by analyzing each pixel line in the diffraction spots on the detector separately to exploit the full wavelength-distribution of the VCN beam at PF2 at once (wavelength-multiplexing). Note that the sample-detector distance is usually insufficient to obtain narrower wavelength spectra for

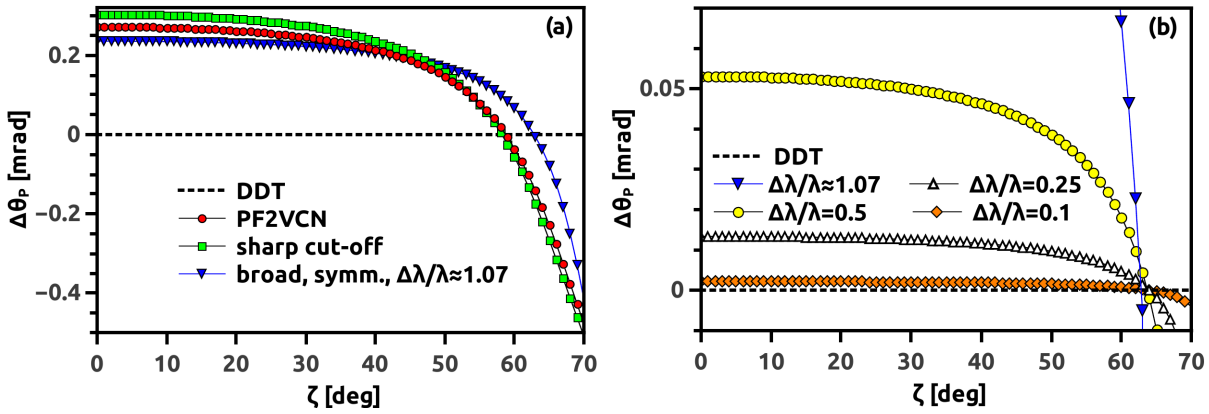

Figure 4. $\Delta\theta_P$ vs. the grating tilt angle ζ for incident spectra of (a) varying asymmetry (see text), (b) various widths $\Delta\lambda/\lambda$.

individual pixel lines, as compared to the width of the incident spectrum. However, the *mean* wavelength is increasing from the top to the bottom pixel line. We found that the intensity loss to absorption/incoherent scattering by an NPC grating is about 20%. To compare this with time-of-flight for PF2VCN in a similar configuration (2 m distance and spectrum ranging from 3 nm to 6 nm with good collimation, say), one suffers at least 80% loss due to the chopper alone. Of course, the wavelength resolution is much better for time-of-flight.

In Fig. 2 (a), one notes that the grating is not mounted in straightforward transmission geometry (also called Laue geometry), but is tilted about the grating vector by the angle ζ. We use such tilt to overcome thickness limitations of NPC gratings or to fine-tune the effective thickness in order to reach a particular reflectivity [33].

In the following section, peculiarities in data analysis that arise due to the VCN incident spectrum are discussed.

3. Appearance of shifted peaks

$\pm1^{\text{st}}$ diffraction order peaks of rocking curves calculated using DDT for a particular NPC grating (parameters: $d = 100\,\mu$m, $b_c\Delta\rho = 4.8\,\mu\text{m}^{-2}$, $\Lambda = 500$ nm) at different tilt angles ζ are shown by the dashed lines in Figs. 3 (a)–(f). The solid, vertical lines are the respective positions of $\pm\theta_B$, which do not depend on ζ. The calculations are carried out for $\lambda = 3$ nm, which is also the mean wavelength of the spectrum shown in Fig. 2 (b). The solid curves are the $\pm1^{\text{st}}$ diffraction order peaks of rocking curves calculated numerically by a convolution of the DDT curves with a slit function (according to the divergence of $\approx$1 mrad in our experiments) and the assumed wavelength distribution as shown in Fig. 2 (b). Taking a closer look at the peak positions $\pm\theta_P$ of the solid curves, one observes slight deviations from $\pm\theta_B$ depending on ζ. While for $\zeta = 0°$ [Fig. 3 (a)] the peak positions $\pm\theta_P$ are larger than $\pm\theta_B$, the former decrease with increasing ζ until $\pm\theta_P = \pm\theta_B$ at $\zeta \approx 59°$ [Fig. 3 (c)], only to be shifted further towards $\theta = 0°$ for higher ζ. For $\zeta = 70°$ [Fig. 3 (f)], one can see that the solid curves become also quite asymmetric.

Though surprising at first sight, it is clear that the shift of θ_P stems from incoherent superposition of the rocking curves measured 'at once' with a wide and asymmetric incident wavelength spectrum: Δn_1 is proportional to λ^2, so the reflectivity is much higher at longer wavelengths. Furthermore, curves for longer λ exhibit larger diffraction angles. Fig. 4 (a) shows deviations $\Delta\theta_P = \theta_P - \theta_B$ (calculated) from the DDT peak-position θ_B as a function of ζ for several different incident wavelength spectra that all exhibit the same mean wavelength of $\lambda_{\text{mean}} = 3$ nm. The horizontal, dashed line is the DDT prediction for a perfectly collimated,

monochromatic incident beam. The filled red circles represent the results for the PF2VCN model-spectrum of Fig. 2 (b) with a width of $\Delta\lambda = 3.2\,\mathrm{nm}$. The filled green squares represent data computed assuming a very sharp wavelength cut-off, for which $\lambda_{\max}$ (the wavelength of highest flux) is at the left border of the distribution. The filled, blue upside-down triangles assume a distribution symmetrical around λ_{mean} with the same large $\Delta\lambda$ as above, which—due to its symmetry—can be characterized by $\Delta\lambda/\lambda \approx 1.07$. The latter data set is also shown in Fig. 4 (b), together with data extracted from simulations assuming symmetrical distributions with decreasing values of $\Delta\lambda/\lambda$. In particular, further data are shown for $\Delta\lambda/\lambda = 0.5$ (filled yellow circles), $\Delta\lambda/\lambda = 0.25$ (empty triangles) and $\Delta\lambda/\lambda = 0.1$ (filled orange squares). Inspecting the difference in scaling of the $y-$axes in Figs. 4 (a) and (b), one can infer that the exact form (the asymmetry, in this case) plays a minor role in the shifts of θ_P as compared to the actual width of the incident wavelength distribution.

If the incident mean wavelength is to be estimated only from peak positions and the Bragg condition, the shifts account for errors of up to 10%. With respect to our experimental method (wavelength-multiplexing by line-by-line analysis of diffraction spots) proposed above, it is clear that one cannot obtain a consistent estimation of the mean wavelength incident at a particular pixel line or other parameters aimed at, without taking the above findings into consideration.

Note that even for $\Delta\lambda/\lambda = 0.1$, as is the case of widths of typical SANS incident wavelength-spectra, there is some deviation in θ_P to be expected [Fig. 4 (b)]. However, it would be only of the order of $10^{-3}\,\mathrm{mrad}$ or—translated to wavelengths—$10^{-2}\,\text{Å}$. Note also that the actual maximum tilt angle we have reached in experiments so far is about 80°. The behavior of θ_P in the range $70° \leq \zeta < 90°$ exhibits interesting resonance-like features, which will be discussed elsewhere.

4. Rocking curve shape-imperfection due to attenuation of the grating-strength along the sample depth

As already mentioned, in Ref. [35] an NPC grating was used as three-port beam splitter for neutrons at a wavelength $\lambda = 1.7\,\mathrm{nm}$. Grating parameters deduced were mainly due to an estimation at the Bragg angles, applying a two-beam coupling model [16]. This model, however, is only a rough approximation for two reasons: *(i)* standard two beam-coupling theories must fail as at least the consideration of three beams is vital to assess the situation, *(ii)* the side minima of the rocking curve are obviously lifted from the zero line.

To tackle problem *(i)* it would be sufficient to apply the RCWA [25, 26] by fitting it to the data. As discussed in the previous section, *(ii)* might be caused by a convolution of the wavelength distribution with the rocking curve. While this is important for diffraction measurements using the broad spectrum of PF2VCN, the situation is different for the rather narrow wavelength distribution at the SANS I instrument of PSI ($\Delta\lambda/\lambda \approx 0.1$), where the measurements shown in [35] were performed.

Another well known effect that might lead to *(ii)*, is a nonuniformity of the grating strength along the sample depth [19] like, e.g., attenuation of the grating modulation-amplitude along the grating depth. The tedious task of including such a behavior into the RCWA was performed in Ref. [37] by dividing the hologram in a large number of layers along the sample depth, each of them treated by the RCWA and considering the boundary conditions between subsequent layers. We choose a more pragmatic approach. By inspecting the data shown in Fig. 5 we note that only five diffraction orders $(\pm 2, \pm 1, 0)$ are observed. Therefore, we set up a five-wave coupling theory allowing for a profile of the coupling parameters along the sample depth and solve a set of coupled first-order ordinary differential equations. Second-order derivatives are disregarded (slowly-varying amplitude approximation) as the refractive-index modulation is moderate and reflection of neutrons at the surfaces can be neglected ($n_0 \approx 1$). This procedure gives rise to an ambiguity for the choice of boundary conditions [23, 38, 39, 40, 41]. Here, we opt for the

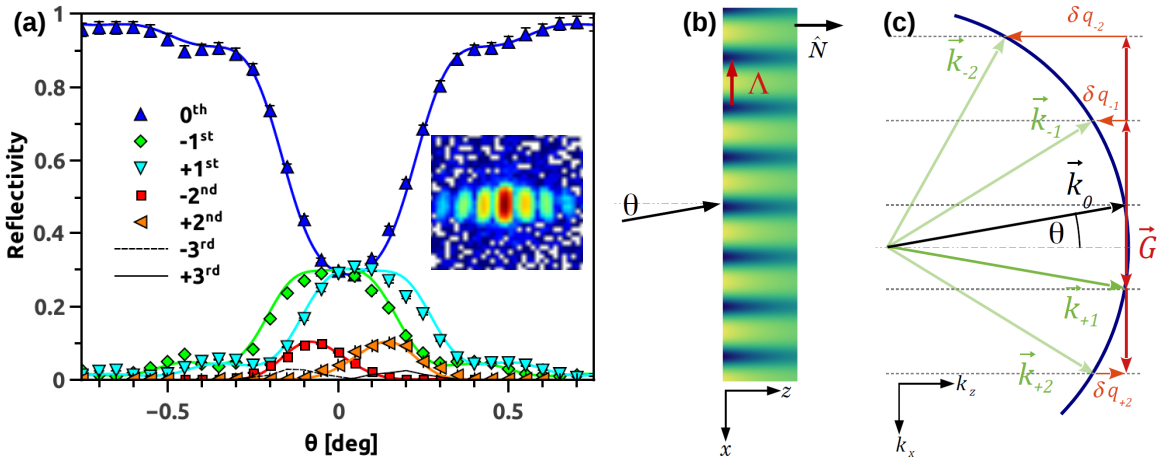

Figure 5. (a) Rocking curve for an NPC three-port beam splitter ($\zeta \approx 56°$). The inset shows a sum of the detector counts for all measured angular positions. (b) Geometrical configuration of a $x-z$-planar diffraction grating. $\vec{G} = G(1,0,0) = 2\pi/\Lambda(1,0,0)$, $\hat{N} = (0,0,1)$. (c) Ewald sphere at Bragg incidence for $+1^{\text{st}}$ order (not to scale), Floquet-condition.

beta-value method (see e.g. [38]), i.e., $|\vec{k}_0| = |\vec{k}_{\pm1}| = |\vec{k}_{\pm2}| = 2\pi/\lambda := \beta$. The system of ODEs is solved numerically to fit it to the experimentally determined reflectivity. We refine the description of the refractive index modulation in our gratings (see Sec. 1) by allowing for an arbitrary profile along the sample depth z [see Fig. 5 (b)]:

$$n(x,z) = 1 + \Delta n_1(z)\cos(Gx) + \Delta n_2(z)\cos(2Gx) + \ldots \tag{1}$$

Here, $\Delta n_i(z)$ are the depth-dependent Fourier-components of the refractive index, $G = 2\pi/\Lambda$ is the modulus of the grating vector (spatial frequency). Neutrons are assumed to travel only in the $x-z$ plane. The wave equation (deduced from the time-independent Schrödinger equation) reads:

$$\left(\nabla^2 + k^2\right)\psi(x,z) = 0, \tag{2}$$

where $k = \beta n(x,z)$ and $\psi(x,z)$ is the wave function. For the latter we use a coupled-wave ansatz $\psi(x,z) = \sum_j S_j(z) e^{-\imath \vec{k}_j \cdot \vec{x}}$, where $S_j(z)$ are the diffraction amplitudes to be determined. The Floquet condition requires that

$$\vec{k}_j = \vec{k}_0 + j\vec{G} - \delta q_j \hat{N}, \tag{3}$$

with the (scalar) mismatch parameter

$$\delta q_j = \beta\left[\cos\theta - \sqrt{1 - (\sin\theta + jG/\beta)^2}\right]. \tag{4}$$

Here, θ denotes the angle between the sample surface normal $\hat{N}$ and the wavevector $\vec{k}_0$ of the incident beam. Inserting Eqs. (1), (3) and (4) into the wave equation (2), disregarding the second order derivatives and sorting the terms according to their propagation directions yields the coupled differential equations to be solved for the $S_j(z)$ with the boundary conditions $S_0(z=0) = 1$ and $S_j(z=0) = 0\ \forall j \neq 0$:

$$\begin{aligned} 2\imath k_{j,z} S_j(z)' &= \beta^2\left[\Delta n_1(z)\left(S_{j+1}(z)e^{\imath(\delta q_{j+1} - \delta q_j)z} + S_{j-1}(z)e^{\imath(\delta q_{j-1} - \delta q_j)z}\right)\right. \\ &+ \left.\Delta n_2(z)\left(S_{j+2}(z)e^{\imath(\delta q_{j+2} - \delta q_j)z} + S_{j-2}(z)e^{\imath(\delta q_{j-2} - \delta q_j)z}\right)\right], \end{aligned} \tag{5}$$

Table 1. Summary of fitting results.

	$\zeta \approx 55°$	$\zeta \approx 0°$
λ	(1.72 ± 0.03) nm	(1.65 ± 0.05) nm
Δn_1^0	$(5.05 \pm 0.10) \times 10^{-6}$	$(5.18 \pm 0.15) \times 10^{-6}$
Δn_2^0	$-(9.4 \pm 0.6) \times 10^{-7}$	$-(1.12 \pm 0.05) \times 10^{-6}$
d	(186 ± 1) μm	(99 ± 1) μm
L	(109 ± 2) μm	(65 ± 1) μm
$\langle b_c \Delta\rho_1 \rangle$	$(5.1 \pm 0.2)/\mu\text{m}^2$	$(6.2 \pm 0.4)/\mu\text{m}^2$
$\langle b_c \Delta\rho_2 \rangle$	$-(0.96 \pm 0.07)/\mu\text{m}^2$	$-(1.3 \pm 0.1)/\mu\text{m}^2$

where we use the abbreviation $S_j(z)' = \partial S_j(z)/\partial z$. The j-th order reflectivity R_j is given by $R_j = k_{j,z}/k_{0,z}|S_j(z=d)|^2$.

4.1. Experimental data and fitting

Rocking curves were measured for two tilt angles ($\zeta \approx 0°, 55°$). As explained in Sec. 2, longer wavelength neutrons hit the detector at lower positions and larger Bragg angles. However, it can be seen from Fig. 5 (inset) that the rather narrow wavelength distribution of SANS I is negligible: the longish diffraction spots are almost vertical and parallel. Therefore, we evaluated the angular dependence of the reflectivity by summing up all the counts of each diffraction spot in contrast to the line-by-line analysis. Next, we assume the functional dependence of the refractive-index depth-profile to be exponential with a decay length L such that $\Delta n_j(z) = \Delta n_j^0 e^{-z/L}$. This is a quite obvious choice as usually light absorption and—as in our case—linear light scattering processes lead to the exponential attenuation of the interference-fringe amplitude along the z-direction during recording [42, 43]. However, our model is not restricted to this particular choice. The profile can be of arbitrary form since the *mean* Fourier components (proportional to the mean values $\langle b_c \Delta\rho_j \rangle$) relate to the Fourier components Δn_j^0 simply by averaging over d (integration along sample depth, Eq. (5) in Ref. [33]).

Using the numerical solutions to Eqs. (5) for five waves ($\pm 2, \pm 1, 0$ diffraction orders), a fit to the rocking curves at two tilt angles ($\zeta \approx 0°, 55°$) yielded the parameters in Tab. 1. Note that the modulation parameters Δn_i^0 and the wavelengths for the two tilt angles are perfectly consistent and the thicknesses are simply related by $d = d(\zeta = 0)/\cos\zeta$. Similar reasoning applies to the decay lengths L [33]. Further, for VCN measurements we have to consider that the coherent scattering-length density modulation amplitudes $b_c \Delta\rho_j$ for the j-th Fourier coefficient are related to the refractive-index modulation amplitudes Δn_j via $b_c \Delta\rho_j = 2\pi/(\lambda^2)\Delta n_j$ and are, thus, wavelength dependent.

The mean wavelength for the measurements at PF2VCN was about 3.6 nm. A sum of counts in detector images at all angles of incidence is shown in the inset of Fig. 6. The skewed diffraction spots in the inset indicate the rather wide wavelength distribution, similar to our model distribution in Fig. 2 (b). In this case, it is mandatory to apply the line-by-line analysis. We employ the same model as in the previous (SANS I) case, using the same values for d and L as obtained from the previous evaluation (Tab. 1). The results obtained for two different horizontal detector lines, i.e., two different mean wavelengths, are shown in Fig. 6.

As expected, the fit to the data becomes worse as the wavelength increases. We attribute this observation to the fact that we did not consider the wavelength spectrum and the beam divergence. A more detailed study on these features is under way.

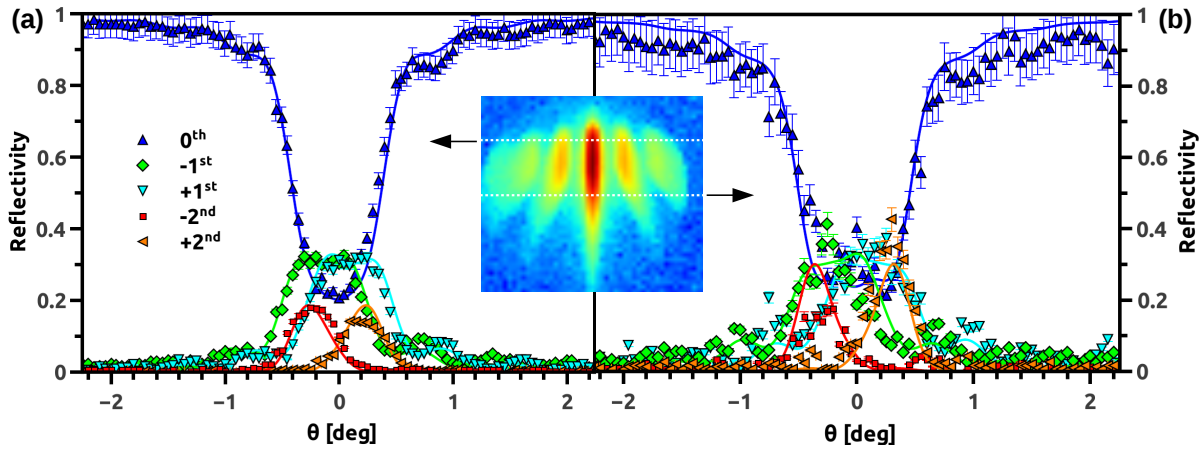

Figure 6. Rocking curves for two different pixel-lines. (a) $\lambda = (3.73 \pm 0.07)$ nm (fit result) and (b) $\lambda = (5.0 \pm 0.1)$ nm (fit result). The inset shows the sum of 2D-detector counts for all measured angles of incidence.

References

[1] Rupp R A, Hehmann J, Matull R and Ibel K 1990 *Phys. Rev. Lett.* **64** 301–302
URL http://link.aps.org/doi/10.1103/PhysRevLett.64.301
[2] Havermeyer F, Lyuksyutov S F, Rupp R A, Eckerlebe H, Staron P and Vollbrandt J 1998 *Phys. Rev. Lett.* **80**(15) 3272–3275
URL http://link.aps.org/doi/10.1103/PhysRevLett.80.3272
[3] Schellhorn U, Rupp R A, Breer S and May R P 1997 *Physica B: Condensed Matter* **234236** 1068 – 1070 proceedings of the First European Conference on Neutron Scattering
URL http://www.sciencedirect.com/science/article/pii/S092145269700015X
[4] Pruner C, Fally M, Rupp R A, May R P and Vollbrandt J 2006 *Nucl. Instrum. Methods A* **560** 598 – 605
URL http://www.sciencedirect.com/science/article/pii/S0168900205026811
[5] Fally M 2002 *Appl. Phys. B* **75** 405
URL http://dx.doi.org/10.1007/s00340-002-1035-0
[6] Fally M, Drevenšek-Olenik I, Ellabban M A, Pranzas K P and Vollbrandt J 2006 *Phys. Rev. Lett.* **97** 167803
URL http://link.aps.org/doi/10.1103/PhysRevLett.97.167803
[7] Fally M, Bichler M, Ellabban M A, Drevenšek-Olenik I, Pruner C, Eckerlebe H and Pranzas K P 2009 *J. Opt. A: Pure Appl. Opt.* **11** 024019
URL http://stacks.iop.org/1464-4258/11/i=2/a=024019
[8] Suzuki N, Tomita Y and Kojima T 2002 *Appl. Phys. Lett.* **81** 4121
URL http://scitation.aip.org/content/aip/journal/apl/81/22/10.1063/1.1525391
[9] Tomita Y, Suzuki N and Chikama K 2005 *Opt. Lett.* **30** 839
URL http://ol.osa.org/abstract.cfm?URI=ol-30-8-839
[10] Chikama K, Mastubara K, Oyama S and Tomita Y 2008 *Journal of Applied Physics* **103**
URL http://scitation.aip.org/content/aip/journal/jap/103/11/10.1063/1.2938849
[11] Tomita Y, Hata E, Momose K, Takayama S, Liu X, Chikama K, Klepp J, Pruner C and Fally M 2016 *Journal of Modern Optics* **63** S1–S31
URL http://dx.doi.org/10.1080/09500340.2016.1143534
[12] Klepp J, Drevenšek-Olenik I, Gyergyek S, Pruner C, Rupp R A and Fally M 2012 *J. Phys.: Conf. Ser.* **340** 012031
URL http://stacks.iop.org/1742-6596/340/i=1/a=012031
[13] Klepp J, Pruner C, Tomita Y, Geltenbort P, Drevenšek-Olenik I, Gyergyek S, Kohlbrecher J and Fally M 2012 *Materials* **5** 2788–2815
URL http://www.mdpi.com/1996-1944/5/12/2788
[14] Fujii R, Guo J, Klepp J, Pruner C, Fally M and Tomita Y 2014 *Opt. Lett.* **39** 3453–3456
URL http://ol.osa.org/abstract.cfm?URI=ol-39-12-3453
[15] Guo J, Fujii R, Ono T, Klepp J, Pruner C, Fally M and Tomita Y 2014 *Opt. Lett.* **39** 6743–6746
URL http://ol.osa.org/abstract.cfm?URI=ol-39-23-6743

[16] Kogelnik H 1969 *Bell System Technical Journal* **48** 2909–2947 ISSN 1538-7305
URL http://dx.doi.org/10.1002/j.1538-7305.1969.tb01198.x
[17] Sears V F 1989 *Neutron Optics* (Oxford, UK: Oxford University Press)
[18] Rauch H and Werner S A 2015 *Neutron Interferometry* (Oxford, UK: Oxford University Press)
[19] Uchida N 1973 *J. Opt. Soc. Am.* **63** 280–287
URL http://www.osapublishing.org/abstract.cfm?URI=josa-63-3-280
[20] Gaylord T and Moharam M 1982 *Applied Physics B* **28** 1–14 ISSN 0946-2171
URL http://dx.doi.org/10.1007/BF00693885
[21] Klepp J, Pruner C, Ellabban M A, Tomita Y, Lemmel H, Rauch H and Fally M 2011 *Nucl. Instrum. Methods A* **634** S59–S62
URL http://www.sciencedirect.com/science/article/pii/S0168900210015779
[22] Fally M, Klepp J and Tomita Y 2012 *Appl. Phys. B* **108** 89–96 ISSN 0946-2171
URL http://dx.doi.org/10.1007/s00340-012-5090-x
[23] Prijatelj M, Klepp J, Tomita Y and Fally M 2013 *Phys. Rev. A* **87**(6) 063810
URL http://link.aps.org/doi/10.1103/PhysRevA.87.063810
[24] Gaylord T K and Moharam M G 1981 *Appl. Opt.* **20** 3271–3273
URL http://ao.osa.org/abstract.cfm?URI=ao-20-19-3271
[25] Moharam M G and Gaylord T K 1981 *J. Opt. Soc. Am.* **71** 811–818
URL http://www.osapublishing.org/abstract.cfm?URI=josa-71-7-811
[26] Moharam M G, Gaylord T K, Grann E B and Pommet D A 1995 *J. Opt. Soc. Am. A* **12** 1068–1076
URL http://josaa.osa.org/abstract.cfm?URI=josaa-12-5-1068
[27] Sippel D, Kleinstueck K and Schulze G 1965 *Physics Letters* **14** 174 – 175 ISSN 0031-9163
URL http://www.sciencedirect.com/science/article/pii/0031916365905706
[28] Shull C G 1968 *Phys. Rev. Lett.* **21**(23) 1585–1589
URL http://link.aps.org/doi/10.1103/PhysRevLett.21.1585
[29] Shull C G 1973 *Journal of Applied Crystallography* **6** 257–266 ISSN 1600-5767
URL http://dx.doi.org/10.1107/S0021889873008654
[30] Somenkov V A, Shilstein S S, Belova N E and Utemisov K 1978 *Solid State Commun.* **25** 593–595
URL http://www.sciencedirect.com/science/article/pii/0038109878914977
[31] Klepp J, Pruner C, Tomita Y, Geltenbort P and Fally M 2016 In preperation
[32] Fally M, Klepp J, Tomita Y, Nakamura T, Pruner C, Ellabban M A, Rupp R A, Bichler M, Drevenšek-Olenik I, Kohlbrecher J, Eckerlebe H, Lemmel H and Rauch H 2010 *Phys. Rev. Lett.* **105** 123904
URL http://link.aps.org/doi/10.1103/PhysRevLett.105.123904
[33] Klepp J, Pruner C, Tomita Y, Plonka-Spehr C, Geltenbort P, Ivanov S, Manzin G, Andersen K H, Kohlbrecher J, Ellabban M A and Fally M 2011 *Phys. Rev. A* **84** 013621
URL http://link.aps.org/doi/10.1103/PhysRevA.84.013621
[34] Klepp J, Pruner C, Tomita Y, Mitsube K, Geltenbort P and Fally M 2012 *Appl. Phys. Lett.* **100** 214104
URL http://scitation.aip.org/content/aip/journal/apl/100/21/10.1063/1.4720511
[35] Klepp J, Tomita Y, Pruner C, Kohlbrecher J and Fally M 2012 *Appl. Phys. Lett.* **101** 154104
URL http://scitation.aip.org/content/aip/journal/apl/101/15/10.1063/1.4758686
[36] Steyerl A, Nagel H, Schreiber F X, Steinhauser K A, Gähler R, Gläser W, Ageron P, Astruc J, Drexel W, Gervais G and Mampe W 1986 *Phys. Lett. A* **116** 347 – 352
URL http://www.sciencedirect.com/science/article/pii/0375960186905876
[37] Neipp C, Sheridan J, Gallego S, Ortuño M, Márquez A, Pascual I and Beléndez A 2004 *Optics Communications* **233** 311 – 322 ISSN 0030-4018
URL http://www.sciencedirect.com/science/article/pii/S0030401804001075
[38] Sheridan J 1992 *Journal of Modern Optics* **39** 1709–1718
URL http://www.tandfonline.com/doi/abs/10.1080/713823578
[39] Kong J A 1977 *J. Opt. Soc. Am.* **67** 825–829
URL http://www.osapublishing.org/abstract.cfm?URI=josa-67-6-825
[40] Yeh P 1993 *Introduction to Photorefractive Nonlinear Optics* Wiley Series in Pure and Applied Optics (New York: Wiley)
[41] Russell P 1981 *Physics Reports* **71** 209 – 312
URL http://www.sciencedirect.com/science/article/pii/0370157381901964
[42] Suzuki N and Tomita Y 2004 *Appl. Opt.* **43** 2125
URL http://ao.osa.org/abstract.cfm?URI=ao-43-10-2125
[43] Suzuki N and Tomita Y 2007 *Appl. Opt.* **46** 6809–6814
URL http://ao.osa.org/abstract.cfm?URI=ao-46-27-6809